Biomaterials 32 (2011) 3547–3554

Contents lists available at ScienceDirect

Biomaterials

journal homepage: www.elsevier.com/locate/biomaterials

In vivo molecular evidence of delayed titanium implant osseointegration in compromised bone

Katleen Vandamme [a,b,*], Xavier Holy [c], Morad Bensidhoum [a], Delphine Logeart-Avramoglou [a], Ignace E. Naert [b], Joke A. Duyck [b], Hervé Petite [a]

[a] Laboratory of Bioengineering and Biomechanics for Bone Articulation (B2OA – UMR CNRS 7052), University Paris Diderot, 10 Avenue de Verdun, 75010 Paris, France
[b] Department of Prosthetic Dentistry/BIOMAT Research Cluster, Faculty of Medicine, Katholieke Universiteit Leuven, Kapucijnenvoer 7, 3000 Leuven, Belgium
[c] Département de Soutien Médico-Chirurgical des Forces, Institut de Recherche Biomédicale des Armées, BP 73, 91220 Brétigny-sur-Orge, France

ARTICLE INFO

Article history:
Received 17 December 2010
Accepted 19 January 2011
Available online 15 February 2011

Keywords:
Titanium
Implant
Osseointegration
Bone
Gene expression
Animal model

ABSTRACT

Optimization of implant osseointegration in patients with reduced bone healing potential is a challenge remaining in implant dentistry. Identification of the genes that are modulated during implant osseointegration in normal *versus* osteopenic bone is needed to successfully address these pertinent clinical needs. The present study aimed to assess the initial and early molecular events following titanium implant installation in normal and compromised bone in a rat tibia model. Peri-implant tissue from a well-defined tissue regeneration compartment was analyzed at 2 and 7 days post-surgery for the expression of select markers of inflammation, angiogenesis, bone resorption and bone formation. Impaired bone was induced by hindlimb unloading and validated using μCT. The essential step of angiogenesis preceding bone regeneration was evidenced for the peri-implant setting in healthy bone. Compromised bone significantly affected the angiogenesis-osteogenesis coupling in the initial phase (2 days post-surgery), with altered expressions of Vegfa and Epas1 coinciding with downregulated expressions of Col1a1, Bmp2, Bmp4, Alpl and Bglap. At 7 days post-implantation, differences between normal and compromised peri-implant bone were no longer observed. This *in vivo* molecular evidence of delayed implant osseointegration in compromised bone reassert modern strategies in implant development, such as surface modifications and bioengineered approaches, to improve implant osseointegration in compromised conditions.

© 2011 Elsevier Ltd. All rights reserved.

1. Introduction

The implementation of titanium implant osseointegration in oral healthcare in the early 1980s [1] has been a pioneering treatment modality for the replacement of missing teeth. As a consequence of the overall high success rate of oral implants [2], this form of treatment has been widely accepted. Peri-implant endosseous wound healing proceeds along the biological phases of inflammation, angiogenesis and osteogenesis, with resident bone cells and recruited bone marrow progenitor cells as participating players [3,4]. While the implant/bone interface has been characterized up to the ultrastructural level [5,6], the molecular activities of the contributing cells determining the tissue response at the implant interface have been much less explored. Only a limited number of studies have assessed the *in vivo* titanium interface at the genetic level in addition to histological and immunohistochemical evaluations. Some studies examined the healing taking place around titanium implants at early time points (1–7 days post-surgery) [7–10], whereas others at later ones (>7 days post-implantation) [8,11–14]. The vast majority of the aforementioned studies focused on the beneficial properties of the implant surface on the expression of the bone biomarkers. However, a thorough understanding at the genetic scale of the onset phase of bone regeneration at the implant interface is required prior to the development of strategies to further optimize implant osseointegration.

Although its overall high success rate [2], successful implant osseointegration is not straightforward at anatomical sites and/or pathologies associated with impaired bone healing ability such as diabetes, irradiated bone and osteoporosis [15–17]. In an attempt to achieve enhanced biological performance of bone implants in such compromised bone conditions, second generation implants with

* Corresponding author. BIOMAT Research Cluster, Department of Prosthetic Dentistry, School of Dentistry, Oral Pathology and Maxillofacial Surgery, Katholieke Universiteit Leuven, Kapucijnenvoer 7, 3000 Leuven, Belgium. Tel.: +32 16 332438; fax: +32 16 332409.
E-mail address: katleen.vandamme@med.kuleuven.be (K. Vandamme).

0142-9612/$ – see front matter © 2011 Elsevier Ltd. All rights reserved.
doi:10.1016/j.biomaterials.2011.01.056

chemical and micro-structural modifications of the material surface were developed. The decisive role of the implant surface properties on molecular interactions, cellular function and bone regeneration has been demonstrated extensively in *in vitro* research [18]. However, *in vivo* evidence from randomized controlled clinical trials is lacking that these implants have an enhanced clinical performance compared to the machined ones used earlier, in particular in impaired bone conditions [18]. Furthermore, whether, and to what extent the various biological events following implant installation are affected by the host bone properties remain to be determined. In particular the initial phase of implant osseointegration is worth investigating, as e.g. compromised osteoporotic bone has been shown to impede the early phase of osseointegration [19–21]. Acquiring this knowledge will be beneficial in designing customized bioengineered strategies to stimulate bone regeneration at the bone-implant interface in patients with deficient bone healing potential.

The objective of the present study was to assess the initial and early molecular events following titanium implant installation in normal and compromised bone in an animal model. Titanium implants featured by a tissue regeneration compartment were installed in the rat tibia. Impaired bone was induced by hindlimb unloading. Molecular analyses of peri-implant tissue at 2 and 7 days post-surgery addressed the expression of select markers of inflammation, angiogenesis, bone resorption and bone formation. The status of ostepenia and implant osseointegration was further evaluated using micro-CT imaging and histology respectively.

2. Materials and methods

2.1. Rat hindlimb unloading

Forty adult female Wistar rats (Janvier, Le Genest-St-Isle, France) at 14 weeks of age were used and divided into 4 groups. Two groups consisting of 10 animals each were subjected to hindlimb unloading (HU) by tail suspension for a total of 9 (HU-1) or 14 days (HU-2). Another two groups of 10 rats each were weight bearing normally and served as control (CTL) for the HU groups (CTL-1 and CTL-2 respectively). Skeletal unloading was performed as described by Holy and coworkers [22]. Briefly, a tape was applied to the surface of the tail to set a metal clip. The end of the clip was fixed to the overhead bar of a specifically designed Plexiglass cage (400 × 300 × 220 mm; CERMA-Biomeca, France). The height of the bar was adjusted to maintain an approximately 30° head-down tilt with the hindlimbs elevated above the floor of the cage. Rats were allowed to move within the cage using their forelimbs while their hindlimbs were kept free of weight bearing. The CTL animals were housed individually under the same conditions but without tail suspension for the same duration. All rats were kept under controlled animal care conditions at 24 °C under a 12 h light/12 h darkness per diem cycle, fed with standard laboratory chow containing 1% calcium and 0.8% phosphorus (SAFE, Augy, France) and allowed tap water ad libidum. Animals were weighed at the start of and daily during the study. Using video monitoring, two tail suspended rats of the HU-1 group were observed for 24 h for evaluating animal adaptation and behavior. At the end of the experiment, the animals were sacrificed with an overdose of pentobarbital (Doléthal®, Vétoquinol, Lure, France). All experiments were conducted according to institutional guidelines for animal welfare; the animal experimental protocols were approved by the local Ethical Committee for Animal Experimentation.

2.2. Experimental implant

An implant model, recently developed by Vandamme and coworkers [23] was used for assessment of titanium implant osseointegration at the molecular level. In brief, the titanium cylindrical one-piece percutaneous implant (2 × 8 mm) (GC Corporation, Tokyo, Japan) (Fig. 1) consists of a screw-threaded and a threadless part. The screw threads located at both ends of the endosseous part of the implant are in contact with the upper and lower cortical bone and ensure primary implant stability. The middle region of the endosseous part is featured by a threadless cavity of 3.77 mm^3. Regenerated bone tissue can be harvested from this section of the implant (hereafter referred to as 'tissue regeneration area', TRA). The surface topography of the implants was characterized by scanning electron microscopy (SEM Quanta™ 200, FEI, Lyon, France; EDS, Oxford Instruments, Oxfordshire, UK) (Fig. 1).

Implants were installed unilaterally in the tibia of rats of both HU and CTL groups, 7 days after either onset of skeletal unloading or normal weight bearing. In 6 animals (specifically, 3 from the HU-2 and 3 from the CTL-2 group), an implant was additionally installed in the contralateral tibia for subsequent histological processing. Surgery was performed under general anaesthesia. The animals were anesthetized by subcutaneous injection of medetomidine (0.1 mg/kg; Domitor®, Pfizer, Paris, France) and ketamine (75 mg/kg; Ketamine 500®, Vibrac, Carros, France). A small skin incision on the medial side of the proximal metaphysis of the tibia was made to provide access to the bone. Landmarking of a standardized implant positioning was performed by perforating the cortical bone with a sharp probe 5 mm distally from the proximal end of the tibia, centrally in the medio-proximal plateau of the tibia. A bi-cortical cavity with a diameter of 1.75 mm was drilled using low rotational speed and continuous irrigation via external saline. Implants were inserted by manual torque; their primary stability was ensured by bi-cortical fixation. The rat leg was splinted with an elastic adhesive bandage (Tensoplast, BSN Medical, Vibraye, France) and was maintained post-operatively for 2 days. Post-surgery, the animals were awakened by subcutaneous administration of an alpha2-antagonist (1 mg/kg; Antisedan®, Pfizer, Paris, France). Analgesics were given by intramuscular injection of meloxicam (0.3 mg/kg; Metacam®, Boehringer Ingelheim, Reims, France) for the next 2 days.

2.3. Micro-X-ray computed tomography (μCT) analysis of tibial bone

For assessment of the bone architectural changes in response to 9 ('1'-groups) and 14 days ('2'-groups) of skeletal unloading, the proximal parts of tibiae without implant of the HU and CTL rats were examined using a desk-top Micro-CT (Skyscan 1172, Skyscan, Aartselaar, Belgium), equipped with an 80 kV X-ray source with camera pixel size of 9 μm. During scanning, the tibias were placed in polyethylene tubes filled with alcohol 75 volume%. Micro-CT images along the midsagital planes in the metaphyseal region of the bones were obtained. The scans resulted in reconstructed 3D data sets with a voxel size of 8.45 μm and were subsequently quantified using CTAn automated image analysis system (Skyscan, Aartselaar, Belgium). To determine the trabecular volume of interest (VOI) in the axial direction, the growth plate was determined as reference (Fig. 2). The region of interest was chosen with its closest edge at 1.00 mm distally from the growth plate and with a height of 3.38 mm (a total of 400 slices). For each transverse slice, the VOI was delineated manually in an as large as possible area of trabecular bone. The registered gray-value images were segmented into binary images using a Gaussian low-pass filter and a fixed threshold (26.7% of maximal gray-scale value) to extract the mineralized bone phase. The bone volume fraction (BV/TV), trabecular thickness (Tb.Th), trabecular separation (Tb.Sp) and trabecular number (Tb.N) were calculated 3D as measurements of trabecular bone mass and its distribution. The trabecular architecture was quantified by calculating the connectivity of the trabecular network (trabecular bone pattern factor, Tb.Pf) and the structure model index (SMI). Low Tb.Pf values reflect better connected trabecular lattices, while high Tb.Pf values are indicative of disconnected trabecular structures. The SMI values provide information regarding the trabecular shape, that is either rod- (SMI = 3) or plate-like (SMI = 0).

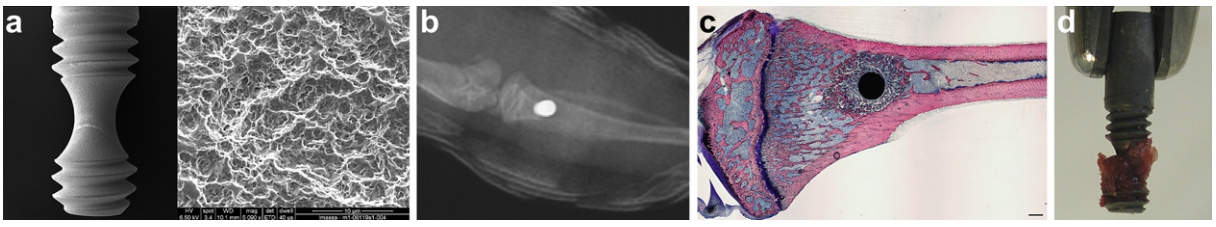


Fig. 1. (a) Implant design and surface characterization (SEM Quanta™ 200, FEI, Lyon, France; EDS, Oxford Instruments, Oxfordshire, UK). The roughened surface (Ra-value of 1.36 ± 0.04 μm) of the pure titanium implants consists of at the micrometer scale relatively smooth structures, irregular in shape but uniformly distributed. (b) Anatomical position of the implant in the rat tibia, visualized by X-ray. (c) Histological section of a 7-days healed implant in a CTL animal, at halfway implant height (cavity) level (Stevenel's blue and von Gieson's picrofuchsin staining; Scale bar = 500 μm). (d) Tissue harvesting from the well-defined peri-implant area.

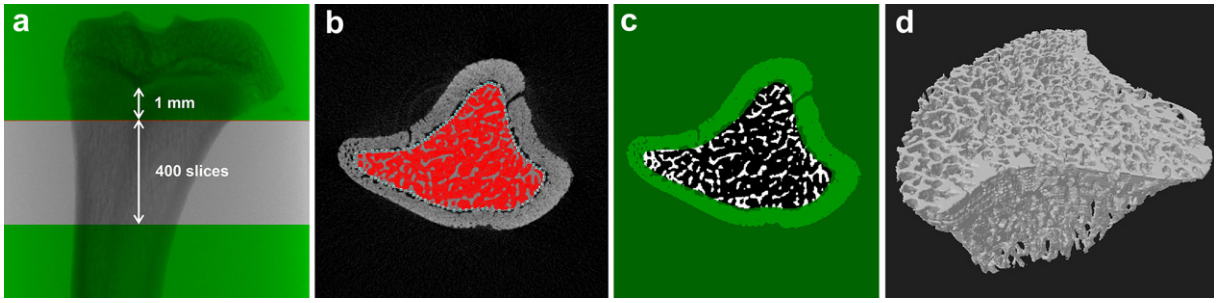
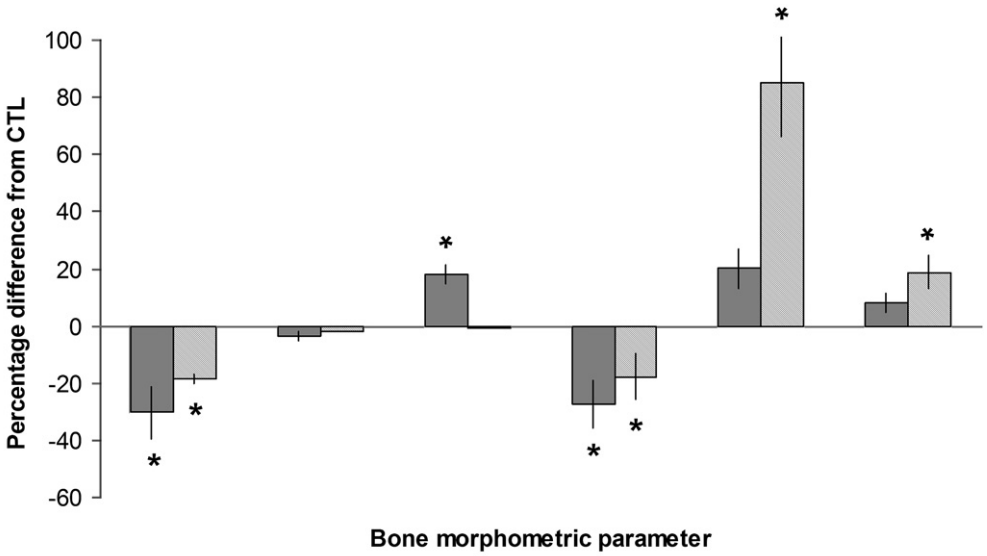


Fig. 2. Representative microtomographic reconstructions of bone slices. (a) Frontal slice of the rat proximal tibia. The investigated site in the axial direction was set at 1 mm distally from the growth plate, with a height of 3.38 mm. (b) On each transversal section, the trabecular bone region of interest was drawn manually a few voxels away from the endocortical surface. The resulting area (2-D) and volume (3-D) of interest are shown (c and d respectively).

2.4. Molecular analysis of peri-implant tissue

Molecular assessment of the initial (i.e., 2 days post-implantation) peri-implant tissue regeneration was performed on samples of 9-days HU and CTL animals (specifically, implants were installed 7 days after the onset of HU/CTL and the peri-implant tissue regenerate was sampled 2 days post-implantation), and of the early (i.e., 7 days post-implantation) tissue response in the animals with a 14-days experimental period (7 days pre- and 7 days post-implantation). The tissue in TRA of the implants was isolated using a befitting trephine burr (PRAXIS, Serris, France). Both cortices were first perforated, where after the implant with attaching tissue was removed manually and immediately immersed in 1 mL of TRIzol (TRIzol® Reagent, Invitrogen, Cergy-Pontoise, France). This procedure was performed under continuous external irrigation and freezing–thawing cycles in liquid nitrogen. Total RNA from the tissue in TRA was extracted according to standard protocols, with an average yield of 9.54 (±4.6) μg per explant. The RNA integrity and purity/concentration were checked using spectrophotometry (Nanodrop 1000, Labtech, Palaiseau, France) and a microfluidics-based platform for RNA analysis (Agilent Bioanalyzer, Agilent Technologies, Massy, France). Random-primed cDNA was synthesized from 500 ng of total RNA using the SuperScript™ II RT Kit (Invitrogen). Equal volumes of cDNA were used to program amplifications through real-time polymerase chain reactions (PCR) using specific primers of genes encoding for hypoxia-inducible factor 1 alpha subunit (Hif1a), vascular endothelial growth factor A (Vegfa), angiopoietin 1 (Angpt1), endothelial PAS domain protein 1 (Epas1), fibroblast growth factor 2 (Fgf2), tumor necrosis factor (Tnf), interleukin 11 (Il11), acid phosphatase 5 tartrate resistant (Acp5), tumor necrosis factor (ligand) superfamily member 11 (Tnfsf11), collagen type I alpha 1 (Col1a1),runt-related transcription factor 2 (Runx2), bone morphogenetic protein 2 (Bmp2), bone morphogenetic protein 4 (Bmp4), bone morphogenetic protein 7 (Bmp7), alkaline phosphatase liver/bone/kidney (Alpl), bone gamma-carboxyglutamate (gla) protein (Bglap), secreted protein acidic cysteine-rich (osteonectin) (Sparc), wingless-type MMTV integration site family member 2 (Wnt2) and 18S (kits TaqMan®, Applied Biosystems inc., Courtaboeuf, France) in the presence of TaqMan Universal PCR Master Mix (Applied Biosystems) using an iCycler thermocycling apparatus (MyiQ™ Single-Color Real-Time PCR; Bio-Rad Laboratories, Marnes-la-Coquette, France). After activation of DNA Polymerase at 95 °C for 10-min, cDNA was amplified by performing 40 two-step PCR cycles: a 15-s denaturation step at 95 °C, followed by a 60-s annealing and extension step at 60 °C. Each sample was run in triplicate. Data were analyzed using MyiQ™ Software (Bio-Rad Laboratories, Marnes-la-Coquette, France). Quantification of gene expression of the 18 different markers monitored was performed using the comparative threshold cycle method (ΔΔCt) with 18S as the endogenous reference.

In addition, the bone marrow of femora from the CTL groups ($n = 5$ animals per group) was harvested. The flushed cell suspensions from each group were reduced to two pools of cells for each group. RNA isolation and subsequent PCRs were performed following the aforementioned procedures.



	BV/TV	Tb.Th	Tb.Sp	Tb.N	Tb.Pf	SMI
HU-1	**-30.3**	-3.4	**18.3**	**-27.5**	20.1	8.2
	p=0.026	*p*=0.155	*p*=0.019	*p*=0.024	*p*=0.155	*p*=0.150
HU-2	**-18.5**	-1.7	-0.7	**-17.7**	**84.4**	**18.8**
	p=0.048	*p*=0.269	*p*=0.457	*p*=0.037	*p*=0.038	*p*=0.031

Fig. 3. Percentage change (±SEM) of the bone morphometric parameters of HU-1 (9-days of hindlimb unloading) and HU-2 (14-days of hindlimb unloading) rats. Significant differences with respect to CTL animals (F-test and Student's *t*-test (one-tailed), $p < 0.05$) are indicated by * on the figure and in bold in the %-change table (the accompanying *p*-values are given). Dark gray bars, HU-1; Light gray bars, HU-2.

2.5. Histological analysis of peri-implant tissue differentiation and bone formation

To evaluate tissue differentiation and bone formation in the vicinity of and in apposition onto the surface of 7-day healed implants, 3 specimens each of the HU-2 and of the CTL-2 group were prepared for histological analysis. Tissue blocks containing the implants were fixed in a $CaCO_3$-buffered formalin solution and dehydrated using series of increased ethanol concentrations over 15 days. Embedding was performed by infiltration of a benzoylperoxide (0.018%)–methylmetacrylate solution over 8 days. Sectioning transversely perpendicular to the implant and grinding were performed using a diamond saw. Seven sections were obtained from each implant and were reduced to a final thickness of 20–30 μm by micro-grinding and polishing using a cutting–grinding device (Exakt 400 CS, Exakt Technologies Inc., Chailly en Bière, France). These sections were stained using a combination of Stevenel's blue and von Gieson's picrofuchsin according to standard techniques. Histological examinations were performed using light microscopy (Olympus BH-2, OSI, Paris, France; Sony Color Camera 3CCD, Sony Business Europe Hampshire, UK).

2.6. Statistical analysis

The μCT and gene expression data were analyzed using the Fischer and Student's *t*-tests and the non-parametric Mann–Whitney test to assess the statistical significance of comparisons between corresponding groups. *P*-values were considered significant when < 0.05.

3. Results

3.1. Validation of the compromised bone-implant model

Video monitoring provided evidence that the animals adapted to the experimental conditions of the present study. The HU apparatus allowed all animals functions. A slight weight loss ($2.0 \pm 1.2\%$) was seen at 1 day post-surgery in all groups. An overall moderate increase in body weight ($10.9 \pm 3.7\%$) was recorded, without significant differences between the respective HU and CTL groups at the end point of the experiments.

Hindlimb unloading negatively affected the trabecular bone volume and the number of trabeculae for both experimental terms (Fig. 3). Furthermore, short-term disuse (9 days; HU-1) affected the spatial distribution of the trabeculae, whereas medium-term hindlimb unloaded tibiae (14 days; HU-2) resulted in a shift towards disconnection of the trabeculae, accompanied by a change to a rod-like morphology.

In the 2-days healed implant groups, all except one implant were bicortically installed with a good primary stability. Neither infection nor bone fracture or implant mobility could be observed at the time of implant retrieval. In the 7-days healed implant groups, fracture of the lower cortical bone occurred once during implant surgery in the HU group. Furthermore, one HU-2 animal automutilated the tail and eventually unplugged the suspension apparatus. One animal of the CTL-2 group died during surgery. The latter two animals were excluded from the study. This action resulted in 9 animals each for the HU-2 and CTL-2 groups, with 8 and 9 samples for molecular assessment respectively.

3.2. Molecular events during implant osseointegration in healthy bone

In an attempt to investigate the osseointegration process occurring in normal bone at the molecular level, the peri-implant gene expression data of the CTL groups were normalized to the

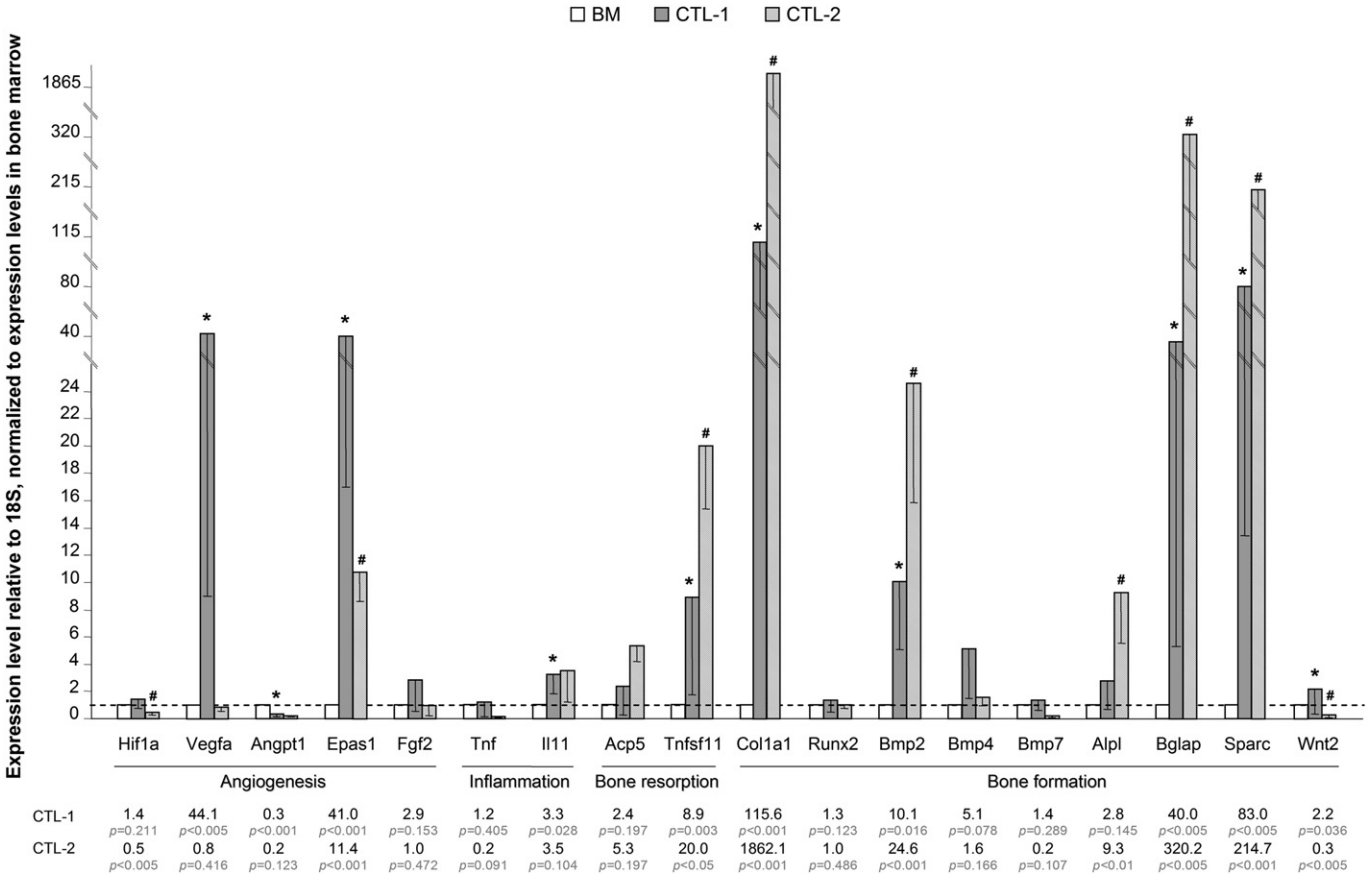


Fig. 4. Gene expression values (mean ± SD) in peri-implant tissue from control rats at 2-days (CTL-1: $n = 10$) and 7-days (CTL-2: $n = 9$) post-implantation. The mRNA levels were related to levels of 18S endogenous reference gene and normalized to the expression levels in the bone marrow. Significant differences (Fischer and Student's *t*-test, $p < 0.05$) with the expression level in the bone marrow cells are indicated by * and # for the 2-days and 7-days post-surgery groups respectively (the accompanying data-table is shown). BM, bone marrow. White bars, BM; Dark gray bars, CTL-1; Light gray bars, CTL-2.

respective expression levels in the bone marrow tissue. This approach was based on the assumption that, owing to the implant bone chamber design and its implantation site, the cells contributing to the osseointegration process mainly originated from the bone marrow. Such data normalization enabled assessment of the effect of titanium implant installation on the gene expression levels of the TRA osteoprogenitor cells (Fig. 4).

The initial phase (2 days post-operatively) of peri-implant wound healing was characterized by an overall upregulation of the gene markers tested. Important significant upregulations occurred for the angiogenic markers Vegfa and Epas1, accompanied by upregulations for some of the bone formation markers (Col1a1; Bglap; Sparc). At 7 days post-operatively, fewer genes were upregulated in the peri-implant tissue, with a clear shift towards increased upregulations of the bone formation markers Col1a1, Bmp2, Alpl, Bglap and Sparc.

3.3. Effect of compromised bone on implant osseointegration

In order to investigate the impact of compromised bone on the gene expression levels of the cells, the data from HU peri-implant regenerating tissue were normalized to the respective expression levels of the CTL animal group. Impaired bone conditions significantly affected angiogenesis-related (specifically Vegfa and Epas1) and bone formation-related factors (specifically Col1a1, Bmp2, Bmp4, Alpl and Bglap) during initial (2 days post-implantation) titanium implant osseointegration (Fig. 5a). Such differences were not evident during the early stage (7 days post-implantation) of the osseointegration process (Fig. 5b). Only Wnt2 – which was not affected in the initial phase – was downregulated during this later healing phase in compromised bone. Alterations in the expression of inflammation-related and bone resorption-related markers were not observed for both time points.

The aforementioned molecular findings at 7-days post-surgery were corroborated by histology (Fig. 6). No qualitative differences in the regenerating tissue explants of normal *versus* compromised bone could be detected. Newly formed tissue consisting of fibrovascular stroma with trabecular bone was observed in the peri-implant cavity. Bone formation in TRA occurred exclusively via a primary repair sequence, without a cartilaginous intermediary. A gradual decrease of TRA bone occupancy and bone-to-implant contact, and increase in neo-formation of blood vessels and bone trabeculae was observed with increasing distance from the host bone. There was no bone in contact with the implant at the sites with the largest host bone-implant bridging distance.

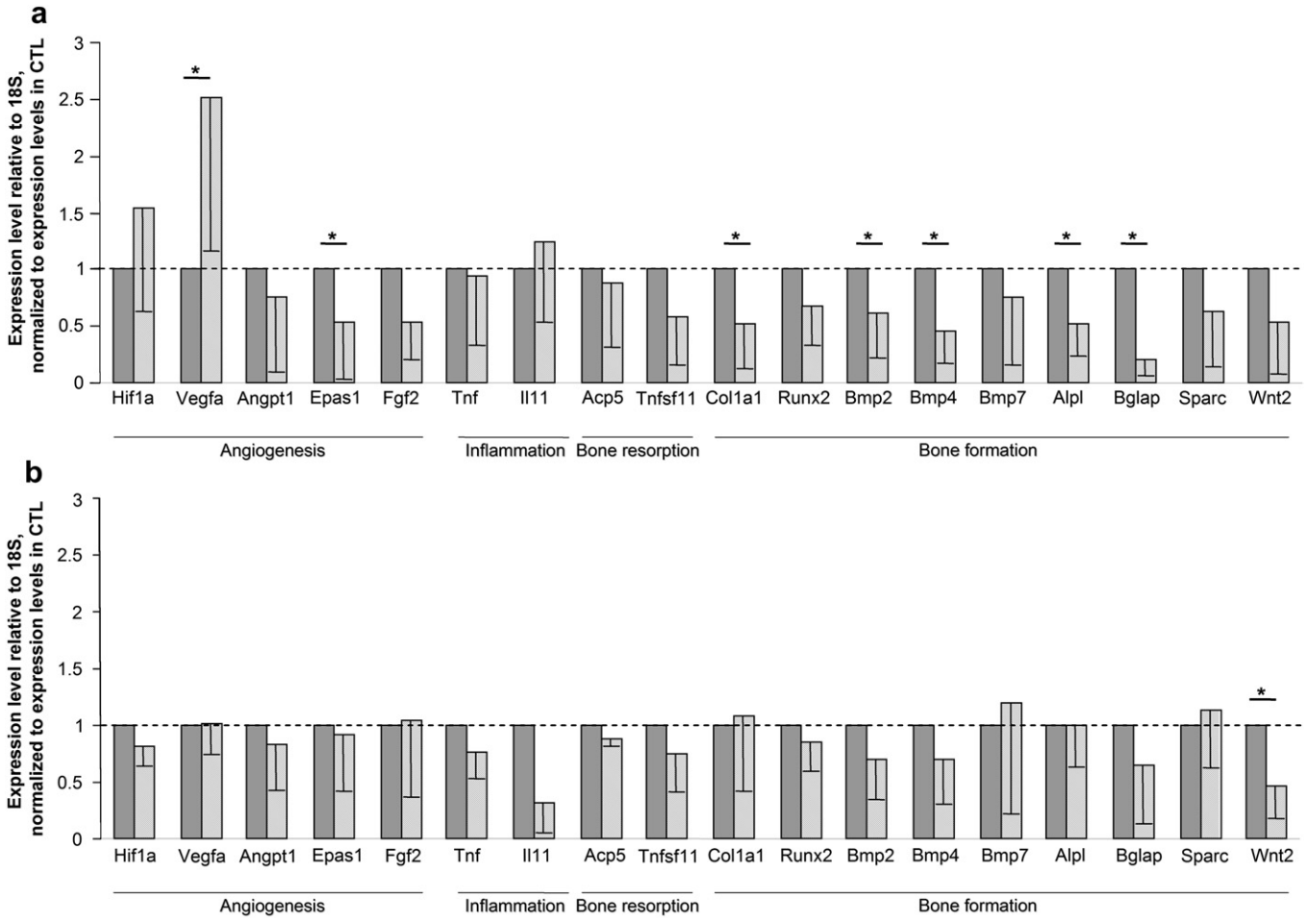


Fig. 5. (a). Gene expression levels (mean ± SD) in 2-days post-implantation peri-implant tissues from control (CTL-1; $n = 10$) and hindlimb unloaded (HU-1; $n = 10$) rats. The mRNA levels in the HU group were standardized to levels of 18S endogenous reference gene and normalized to the respective levels of the CTL group. * indicates significant differences between the groups (Mann–Whitney test, $p < 0.05$). Dark gray bars, CTL-1; Light gray bars, HU-1. (b). Gene expression levels (mean ± SD) in 7-days post-implantation peri-implant tissues from control (CTL-2; $n = 9$) and hindlimb unloaded (HU-2; $n = 8$) rats. The mRNA levels in the HU group were standardized to levels of 18S endogenous reference gene and normalized to the respective levels of the CTL group. * indicates significant differences between the groups (Mann–Whitney test, $p < 0.05$). Dark gray bars, CTL-2; Light gray bars, HU-2.

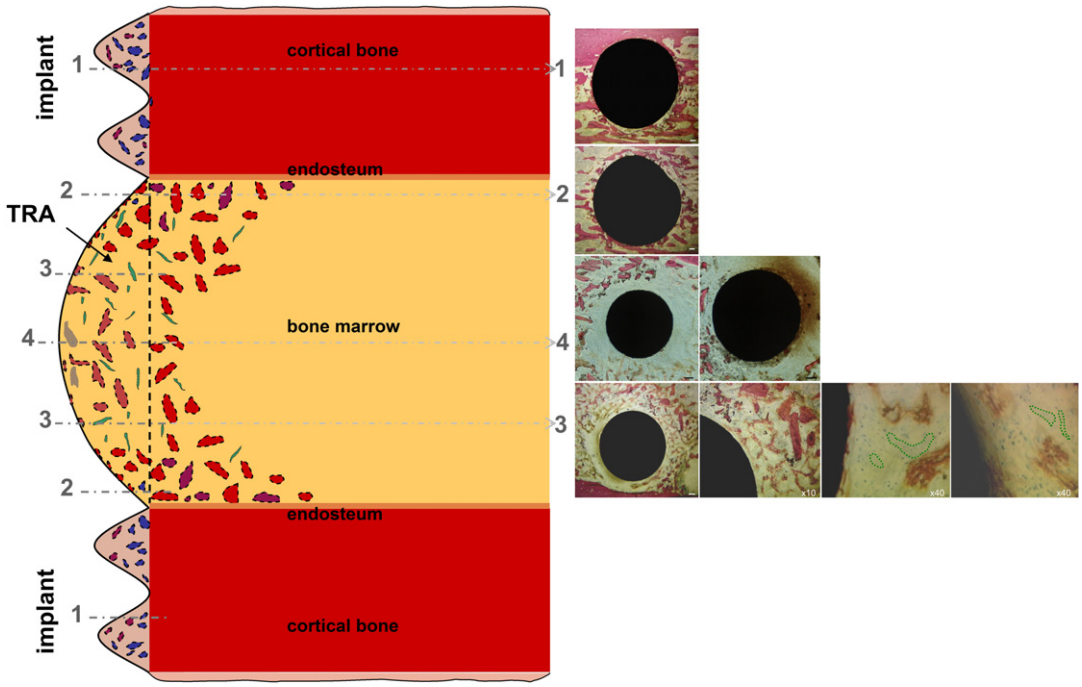


Fig. 6. Schematic representation of the histological observations of a 7-days healed implant (left), with representative illustrations (right). At the cortical bone level (i.e., implant screw thread level) (level 1), bone resorption with primordially necrotic bone remnants (dark blue) and some bone trabeculae under remodeling (blue-red striped) were observed. Bone was in direct contact with the implant screw thread extremities. In the distal region (level 2) of the tissue regenerating area (TRA – half-moon shaped; the dotted line indicates the drill hole width), a considerable amount of bone tissue was in direct contact with the implant (plain red), originating from the endosteal cortical trabeculae (appositional growth) and extending downwards. At the level of increased discrepancy between the implant diameter and the ablation size (level 3), neoformation of blood vessels (green – green dotted lines on the histological sections) and of bone trabeculae (patterned red) was observed, circumferentially around the implant. Bone-to-implant contact was established at discrete locations. In the middle region of TRA (level 4), organized connective tissue was observed around the implant, with signs of tissue differentiation. On some sections, hemosiderin deposits (gray speckled) could be seen, suggesting that hemorrhage due to red blood cells lysis and hemoglobin release had occurred. Bone-to-implant contact occurred rarely at this level. Scale bars = 100 μm.

4. Discussion

Because optimized implant osseointegration in patients with reduced bone healing potential remains one of the challenges in implant dentistry, identification of the genes that are modulated during the establishment of osseointegration is needed to understand and successfully address pertinent clinical needs. Building on experiences with implant osseointegration in the rat tibia model [23], we studied and found that the bone formation-related as well as the preceding angiogenesis-related molecular signals are differentially up- and downregulated during *in vivo* titanium implant osseointegration in normal *versus* compromised bone. A delay in titanium implant osseointegration in compromised host bone was observed.

The hindlimb unloading model was used for exploring osseointegration of titanium implants in the proximal tibial bone. This experimental model is characterized by adversely affected bone quantity and quality [24]. Disuse osteopenia was validated through μCT imaging of the tibiae without implant. The results of the present study support the data of studies in the literature which reported bone architectural alterations in hindlimb unloaded rats [25,26]. In contrast, smaller changes in the trabecular bone volume and trabecular number in response to hindlimb unloaded were recorded in 14 days unloaded rats compared to 9 days unloaded rats. This result can be attributed to a higher body weight at start (+13.9%) of the rats belonging to the 14-days group compared to the 9-days hindlimb unloaded rats. As the two groups were performed successively (and not in parallel; a situation necessitated by the limited availability of the hindlimb unloading cages), random allocation of all animals was not possible.

Motivated by recent literature reports that the bone marrow mesenchymal cells participate in wound healing and implant osseointegration [4], we first tested the associated *in vivo* molecular events in these cells originating from healthy bone in conjunction with implant installation. In the initial healing phase, implant installation induced striking expression level increases of the angiogenic genes Vegfa and Epas1, accompanied by upregulations of the genes Col1a1 and Sparc, which are associated with bone marrow mesenchymal stem cells [27]. Angiogenic alterations were absent in the later healing phase and were replaced by synchronized upregulation of bone formation makers. These observed sequential biological phases taking place in the implant surroundings are indicative for a normal bone wound healing cascade. Moreover, the results confirm the pivotal contribution of neovascularization for triggering bone regeneration and corroborate the findings of Uchida and coworkers [28] on the temporal expression of Vegfa during bone healing.

Secondly, we investigated the impact of osteopenic host bone on the peri-implant gene expression levels. To this end, the data of the HU peri-implant regenerating tissue were normalized to the respective expression levels in CTL peri-implant regenerating tissue. The present study provided evidence that the establishment of implant osseointegration in compromised host bone was affected at both its angiogenic and bone forming phases. The importance of angiogenesis in the process of peri-implant bone formation, and in associated biomaterial optimizations, is gaining importance [29,30]. To date, however, hardly any attention has been given to the *in vivo* study of the role of new blood vessel formation during implant wound healing in compromised bone.

While it has been established that hindlimb unloading alters tissue perfusion patterns in rodents [31,32], the effects of unloading on blood flow to a wounded area have not been reported yet. The observed trend of increased Hif1a expression ($p = 0.082$) during the initial phase of implant integration in HU host bone indicates a hypoxic environment and corroborates the Vegfa upregulation. Delayed revascularization and/or impaired perfusion in the wound area may be responsible for the rise in Vegfa expression in the HU peri-implant regenerate. The contrariety in Hif1a and Epas1 expressions requires further proteomic approaches to identify the angiogenic factors secreted at the interface of an implant installed in normal *versus* compromised bone.

In addition to the angiogenic changes occurring at the earliest time point of the osseointegration process, a downregulation of the osteogenic markers in the HU peri-implant regenerative tissues was observed. The various phases of bone tissue regeneration (inflammation, angiogenesis and bone resorption and formation) which are coordinated in sequence in normal bone seem to be disorganized during the initial step of implant osseointegration in disuse osteoporotic bone. This result may be due to Vegfa failure to instantly stimulate osteoprogenitor cell migration and differentiation [33,34]. It is also likely that the absence of mechanotransductive signaling owing to skeletal unloading negatively affected the osteoblastic differentiation of the participating bone marrow cells in peri-implant healing [35].

After 7 days of healing, expression of all except one biomarker in normal and in compromised peri-implant regenerating tissue was similar. The observed downregulated expression of Wnt2 in the HU regenerate suggests a mechanical signaling-related effect on the osteogenic cell's response [36], which requires further research. Histology confirmed formation of bone at implant surfaces installed in the rat tibia with kinetics in accordance to the literature [37]. Peri-implant bone formation seemed to be interplay between the osteoconductivity property of titanium and the bone forming capacity of resident and newly recruited cells. Potential quantitative (amount) and qualitative (biomechanical properties) differences of the newly formed peri-implant bone of HU *versus* CTL animals were however not explored owing to the limited number of samples.

5. Conclusions

The results of the present study provide *in vivo* molecular evidence of the implant osseointegration cascade and of the impact of the host bone properties herein. We believe that the angiogenic events are crucial for the subsequent implant osseointegration. This requirement is strengthened by the finding that the gene expression of angiogenic markers is differently regulated in normal *versus* compromised bone at 2 days after implantation; this event coincides with a negatively affected osteogenic cell response and results in a suspended implant osseointegration in compromised bone. These results reassert current strategies in implant development to improve implant osseointegration in compromised conditions through bioengineered approaches such as delivery of angiogenic and osteoinductive growth factors.

Source of funding

This work was supported by the Research Fund of the Katholieke Universiteit Leuven (KUL, Belgium – OT/07/059), the Research Foundation – Flanders (FWO) and the French Institute for Dental Research (IFRO, France). The implants were kindly provided by the GC Corporation, Tokyo, Japan.

Acknowledgements

The authors are especially thankful to C. André, L. Begot, X. Butigieg and S. Renault (Institut de Recherche Biomédicale des Armées) for their excellent technical support and assistance.

Appendix

Figures with essential colour discrimination. Certain figures in this article, particularly Figs. 1 and 2 are difficult to interpret in black and white. The full colour images can be found in the online version, at doi:10.1016/j.biomaterials.2011.01.056.

References

[1] Albrektsson T, Branemark PI, Hansson HA, Lindstrom J. Osseointegrated titanium implants. Requirements for ensuring a long-lasting, direct bone-to-implant anchorage in man. Acta Orthop Scand 1981;52(2):155–70.
[2] Esposito M, Hirsch JM, Lekholm U, Thomsen P. Biological factors contributing to failures of osseointegrated oral implants. (I). Success criteria and epidemiology. Eur J Oral Sci 1998;106(1):527–51.
[3] Li S, Tu Q, Zhang J, Stein G, Lian J, Yang PS, et al. Systemically transplanted bone marrow stromal cells contributing to bone tissue regeneration. J Cell Physiol 2008;215(1):204–9.
[4] Xu B, Zhang J, Brewer E, Tu Q, Yu L, Tang J, et al. Osterix enhances BMSC-associated osseointegration of implants. J Dent Res 2009;88(11):1003–7.
[5] Meyer U, Joos U, Mythili J, Stamm T, Hohoff A, Fillies T, et al. Ultrastructural characterization of the implant/bone interface of immediately loaded dental implants. Biomaterials 2004;25(10):1959–67.
[6] Bernhardt R, Scharnweber D, Muller B, Thurner P, Schliephake H, Wyss P, et al. Comparison of microfocus- and synchrotron X-ray tomography for the analysis of osteointegration around Ti6Al4V implants. Eur Cell Mater 2004;7:42–51.
[7] Guo J, Padilla RJ, Ambrose W, De Kok IJ, Cooper LF. The effect of hydrofluoric acid treatment of TiO_2 grit blasted titanium implants on adherent osteoblast gene expression in vitro and in vivo. Biomaterials 2007;28(36):5418–25.
[8] Mendonca G, Mendonca DB, Simoes LG, Araujo AL, Leite ER, Duarte WR, et al. Nanostructured alumina-coated implant surface: effect on osteoblast-related gene expression and bone-to-implant contact in vivo. Int J Oral Maxillofac Implants 2009;24(2):205–15.
[9] Omar O, Lenneras M, Svensson S, Suska F, Emanuelsson L, Hall J, et al. Integrin and chemokine receptor gene expression in implant-adherent cells during early osseointegration. J Mater Sci Mater Med 2010;21(3):969–80.
[10] Omar O, Svensson S, Zoric N, Lenneras M, Suska F, Wigren S, et al. In vivo gene expression in response to anodically oxidized versus machined titanium implants. J Biomed Mater Res A 2010;92(4):1552–66.
[11] Kojima N, Ozawa S, Miyata Y, Hasegawa H, Tanaka Y, Ogawa T. High-throughput gene expression analysis in bone healing around titanium implants by DNA microarray. Clin Oral Implants Res 2008;19(2):173–81.
[12] Monjo M, Lamolle SF, Lyngstadaas SP, Ronold HJ, Ellingsen JE. In vivo expression of osteogenic markers and bone mineral density at the surface of fluoride-modified titanium implants. Biomaterials 2008;29(28):3771–80.
[13] Ogawa T, Nishimura I. Different bone integration profiles of turned and acid-etched implants associated with modulated expression of extracellular matrix genes. Int J Oral Maxillofac Implants 2003;18(2):200–10.
[14] Ogawa T, Nishimura I. Genes differentially expressed in titanium implant healing. J Dent Res 2006;85(6):566–70.
[15] Vandamme K, Holy X, Bensidhoum M, Logeart-Avramoglou D, Naert I, Duyck J, et al. Establishment of an in vivo model for molecular assessment of titanium implant osseointegration in compromised bone. Tissue Eng Part C Methods; 2010 Nov 22.
[16] Ihde S, Kopp S, Gundlach K, Konstantinovic VS. Effects of radiation therapy on craniofacial and dental implants: a review of the literature. Oral Surg Oral Med Oral Pathol Oral Radiol Endod 2009;107(1):56–65.
[17] Javed F, Romanos GE. Impact of diabetes mellitus and glycemic control on the osseointegration of dental implants: a systematic literature review. J Periodontol 2009;80(11):1719–30.
[18] Mellado-Valero A, Ferrer-Garcia JC, Calvo-Catala J, Labaig-Rueda C. Implant treatment in patients with osteoporosis. Med Oral Patol Oral Cir Bucal 2010;15(1):e52–7.
[19] Palmquist A, Omar OM, Esposito M, Lausmaa J, Thomsen P. Titanium oral implants: surface characteristics, interface biology and clinical outcome. J R Soc Interface 2010;7(Suppl. 5):S515–27.
[20] Ozawa S, Ogawa T, Iida K, Sukotjo C, Hasegawa H, Nishimura RD, et al. Ovariectomy hinders the early stage of bone-implant integration: histomorphometric, biomechanical, and molecular analyses. Bone 2002;30(1):137–43.
[21] Qi MC, Zhou XQ, Hu J, Du ZJ, Yang JH, Liu M, et al. Oestrogen replacement therapy promotes bone healing around dental implants in osteoporotic rats. Int J Oral Maxillofac Surg 2004;33(3):279–85.

[22] Vidigal Jr GM, Groisman M, Gregorio LH, Soares GA. Osseointegration of titanium alloy and HA-coated implants in healthy and ovariectomized animals: a histomorphometric study. Clin Oral Implants Res 2009;20(11):1272–7.
[23] Holy X, Zerath E. The suspension device for hindlimb unloading in the rat–results of a video monitoring study. Stal 1996;21(3–4):177–84.
[24] Globus RK, Bikle DD, Morey-Holton E. The temporal response of bone to unloading. Endocrinology 1986;118(2):733–42.
[25] Bloomfield SA, Allen MR, Hogan HA, Delp MD. Site- and compartment-specific changes in bone with hindlimb unloading in mature adult rats. Bone 2002; 31(1):149–57.
[26] David V, Laroche N, Boudignon B, Lafage-Proust MH, Alexandre C, Ruegsegger P, et al. Noninvasive in vivo monitoring of bone architecture alterations in hindlimb-unloaded female rats using novel three-dimensional microcomputed tomography. J Bone Miner Res 2003;18(9):1622–31.
[27] Silva Jr WA, Covas DT, Panepucci RA, Proto-Siqueira R, Siufi JL, Zanette DL, et al. The profile of gene expression of human marrow mesenchymal stem cells. Stem Cells 2003;21(6):661–9.
[28] Uchida S, Sakai A, Kudo H, Otomo H, Watanuki M, Tanaka M, et al. Vascular endothelial growth factor is expressed along with its receptors during the healing process of bone and bone marrow after drill-hole injury in rats. Bone 2003;32(5):491–501.
[29] Raines AL, Olivares-Navarrete R, Wieland M, Cochran DL, Schwartz Z, Boyan BD. Regulation of angiogenesis during osseointegration by titanium surface microstructure and energy. Biomaterials 2010;31(18):4909–17.
[30] Wernike E, Montjovent MO, Liu Y, Wismeijer D, Hunziker EB, Siebenrock KA, et al. VEGF incorporated into calcium phosphate ceramics promotes vascularisation and bone formation in vivo. Eur Cell Mater 2010;19:30–40.
[31] Colleran PN, Wilkerson MK, Bloomfield SA, Suva LJ, Turner RT, Delp MD. Alterations in skeletal perfusion with simulated microgravity: a possible mechanism for bone remodeling. J Appl Physiol 2000;89(3):1046–54.
[32] McDonald KS, Delp MD, Fitts RH. Effect of hindlimb unweighting on tissue blood flow in the rat. J Appl Physiol 1992;72(6):2210–8.
[33] Street J, Bao M, deGuzman L, Bunting S, Peale Jr FV, Ferrara N, et al. Vascular endothelial growth factor stimulates bone repair by promoting angiogenesis and bone turnover. Proc Natl Acad Sci USA 2002;99(15):9656–61.
[34] Grellier M, Ferreira-Tojais N, Bourget C, Bareille R, Guillemot F, Amedee J. Role of vascular endothelial growth factor in the communication between human osteoprogenitors and endothelial cells. J Cell Biochem 2009;106(3): 390–8.
[35] Kreke MR, Sharp LA, Lee YW, Goldstein AS. Effect of intermittent shear stress on mechanotransductive signaling and osteoblastic differentiation of bone marrow stromal cells. Tissue Eng Part A 2008;14(4):529–37.
[36] Gregory CA, Gunn WG, Reyes E, Smolarz AJ, Munoz J, Spees JL, et al. How Wnt signaling affects bone repair by mesenchymal stem cells from the bone marrow. Ann N Y Acad Sci 2005;1049:97–106.
[37] Masuda T, Salvi GE, Offenbacher S, Felton DA, Cooper LF. Cell and matrix reactions at titanium implants in surgically prepared rat tibiae. Int J Oral Maxillofac Implants 1997;12(4):472–85.